Numerical simulations of combustion in a lean stratified propane-air mixture

By C. Jiménez†, D. Haworth‡, T. Poinsot†¶, B. Cuenot† AND R. Blint‖

Direct numerical simulation (DNS) of combustion in globally lean non-homogeneous propane-air mixtures has been performed for several initial distributions of non-homogeneities. Results have shown a strong influence of the scale and asymmetry of this distribution on both the combustion efficiency and thermal NO production, in accordance with experimental results. The simulations also have made possible a quantitative assessment of flamelet modeling for the primary flame, which yielded remarkably good results.

1. Introduction

In direct-injection engines, liquid fuel is injected directly into the combustion chamber to generate a highly stratified fuel/air mixture at ignition time. This has the potential to significantly improve the engine performance, especially at low-speed light-load operation (Takagi, 1998), and is the subject of intense research for both spark-ignition gasoline (Zhao *et al.*, 1999) and compression-ignition Diesel (Krieger *et al.*, 1997) engines.

This flame propagating into a non-homogeneous mixture is a first example of partially premixed combustion, in which the reactants are not completely mixed nor completely separated before combustion and for which modeling can not be based on the traditional premixed/non-premixed combustion scenarios. A second example can be found in aircraft engines, in which fuel and secondary air are injected at various locations, resulting in a nonuniform equivalence ratio at the flame front (Légier *et al.*, 2000).

Research in the field of partially premixed combustion has shown contradictory results concerning the propagating speed and efficiency of a flame in non-homogeneous premixed conditions as compared to the equivalent (in the sense of containing the same amount of fuel and air) uniformly premixed case. The experimental results of Zhou et al., 1998 suggest an enhanced heat release related to the presence of non-homogeneous pockets of rich/lean mixture for a wide range of variation of the parameters of the experiment. On the other hand, theoretical (Peters, 2000) and numerical (Hélie & Trouvé, 1998) results predict exactly the opposite behavior.

One of the motivations of the present project was to try to resolve such contradictions. Results of previous work (Poinsot *et al.*, 1996, Haworth *et al.*, 2000a, Haworth *et al.*, 2000b) had suggested that both the distribution of inhomogeneities in the equivalence ratio space and its spatial length scales would play a major role in increasing/decreasing global heat release, which can in part explain the discrepancies above.

A second objective was to contribute to the modeling of partially premixed combustion.

† CERFACS
‡ Pennsylvania State University
¶ IMFT
‖ GM

Previous studies have shown that in partially premixed systems, combustion occurs in two stages:

- A primary flame is first established that consumes all primary fuel and produces most of the heat release. It is expected that it can be described using a progress variable and laminar flamelet concepts.
- A secondary reaction zone appears behind when fuel fragments from the rich zones, oxidizer from the lean zones, and combustion products mix. There is still controversy on whether it can be seen as a diffusion flame and described by diffusion flamelets or should be described as distributed combustion.

Moreover, the issue of pollutant formation had to be addressed, as higher peak temperatures can increase the pollutant emission level of a stratified lean-charge engine as compared to a homogeneous lean-charge engine (Takagi, 1998). Formation of pollutants such as NO in premixed systems is most commonly computed by adopting equilibrium and steady-state hypotheses that permit postprocessing of production rate as a function of local N_2 and O_2 concentration and temperature (Glassman, 1987). An assessment of the validity of this approach in the present partially premixed case was needed, and for that reason a full thermal NO mechanism was included in this study.

The approach adopted is to perform DNS of a premixed flame propagating into non-homogeneous propane-air mixtures at conditions that approximate the gasoline direct injection (GDI) engine operating conditions in part-load, low-speed operation (Haworth *et al.*, 2000a). A detailed reaction mechanism based in 30 species and 76 reactions (including thermal NO chemistry), multicomponent molecular transport of species, and full resolution of both the turbulent and the chemical scales permits reliable simulations from which information relative to characterization and modeling of these systems can be extracted.

2. Numerical simulation

DNS of a compressible multi-component gas mixture evolving under turbulent velocity conditions is used to perform this study. The conservation equations for mass, momentum, chemical species mass fractions, and energy are solved using the NTMIX-CHEMKIN code (Baum *et al.*, 1994). High-order space and time integration of the equations is performed by sixth-order compact finite-differences (Lele, 1992) and a third-order Runge-Kutta temporal scheme. The elementary reaction production terms and multicomponent molecular transport coefficients are computed using the CHEMKIN and TRANSPORT packages (Kee *et al.*, 1980, Kee *et al.*, 1983).

DNS is extremely expensive. On one hand, a large number of species mass fractions is needed if one wants to represent realistically the chemistry and transport; on the other hand, very fine spatial and temporal grids are needed if the turbulence and chemistry are to be resolved without modeling in order to capture the smallest scales. This results in a severe limitation of the size of the systems that can be simulated if computations are to be performed at affordable costs. The flame width given by the present chemistry is of the order of 0.15 mm, which imposes a minimum size for the computing domain, but much larger sizes are needed to attain realistic turbulent length scales. A three-dimensional simulation of a cubic domain only a few millimeters on each side with the present chemistry would demand CPU times of the order of years. A two-dimensional simulation of the present chemistry in a planar domain a few millimeters on each side requires CPU times on the order of 2-3 days on a NEC SX-5 computer. Of course some turbulent features

are lost in the two-dimensional approximation, and the present computations would be badly suited to the quantitative characterization of the effects of turbulence on mixing and reaction (not only because of the two-dimensionality but also because of the low Reynolds number). But it is a reasonable choice in the present study where turbulence (2D turbulence) is only used as a means of deforming the flame front and no quantitative correlations between turbulence and the flame are sought.

3. Description of the configuration

The selection of the configuration for the present work was guided by previous results (Haworth *et al.*, 2000a) which had shown no great influence of non-homogeneities on the overall heat release, in contradiction with experiments. Analysis of the phenomena that can affect the overall heat release suggests that four main effects are in competition in non-homogeneous premixed systems:

- First, differences in local reaction rate due to local variations in the equivalence ratio produce a deformation of the flame as segments of flame initially propagating at a uniform speed begin to propagate at different speeds. This effect will in all cases produce an *increase in the flame surface* (or length in 2D) as compared to that of a flame propagating into homogeneous reactants. The magnitude of the increase should depend on the spatial distribution and range of inhomogeneities as well as on laminar flame propagation properties.
- Second, differences in local reaction rate give rise to local variations in heat release per unit flame area. This can contribute to *either an increase or a decrease* in global heat release as compared to the homogeneous case, depending mainly on the distribution of non-homogeneities in equivalence ratio space and flame propagation properties.
- Third, turbulent straining effects usually *decrease locally the reaction rate* as the flame surface tends to be aligned with tangential strain, whose effect is to reduce locally the reaction rates. This may affect the homogeneous and the non-homogeneous flames differently as the flame-front shape in the former is totally determined by turbulence, while non-homogeneities can change the flame shape as described above.
- Lastly, locally higher/lower temperatures occur in a non-homogeneous flame as compared to a homogeneous one. Diffusion, conduction, and turbulent mixing would then tend to decrease or increase the mean temperature at the flame front, resulting in *lower/higher reaction rates* as compared to the values based on the local stoichiometry and strain rate. For example, a locally higher temperature than that of the unburned reactants could result in burning at local equivalence ratios beyond the flammability limits.

In Haworth *et al.*, 2000a, results for a *stoichiometric initially laminar flame* propagating into a non-homogeneous turbulent mixture were compared to those of a homogeneous mixture having the same amount of fuel/air, that is, *conserved mean stoichiometry*. Locally fuel-lean or fuel-rich regions correspond in this case to lower reaction rates (laminar flame speed peaks at a slightly fuel-rich equivalence ratio; Fig. 1). The resulting reduction in mean heat release per unit flame length approximately compensated for the flame surface increase, yielding essentially the same overall heat release for non-homogeneous and homogeneous flames. Maximum differences were approximately of 10%. Later work (Haworth *et al.*, 2000b) showed that variations in the spatial scales of inhomogeneities have a strong effect due to the change of scale of the flame-front deformations. For example, very small rich/lean pockets are not able to produce an appreciable deformation in the flame front, and thus the net effect is a reduction in heat release.

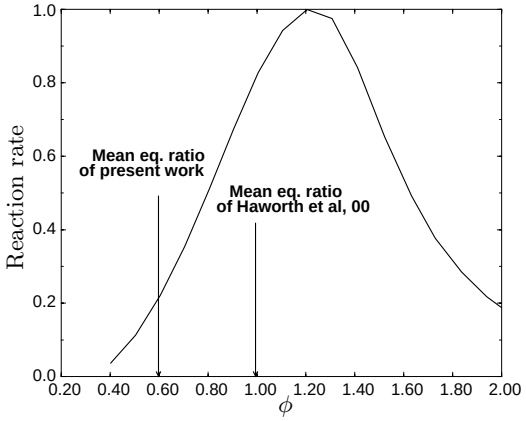

FIGURE 1. Normalized reaction rate of a premixed propane-air laminar flame as a function of equivalence ratio ϕ.

Case	ϕ_{min}	ϕ_{max}	$\langle\phi\rangle$	$\langle\phi'^2\rangle$	λ_ϕ
A Hom.	.6	.6	.6	0	0
B1 Non-hom.	.06	1.14	.6	.15	1
C1 Non-hom.	.03	2.06	.6	.45	1
C2 Non-hom.	.03	2.06	.6	.45	4

TABLE 1. Description of equivalence ratio distributions in the simulations.

L_x, L_y	n_x, n_y	τ_{T0}/τ_f	u'_{T0}/s_l^0	l_{T0}/δ_l^0	Re_{T0}
3 mm	451	.136	11.6	1.58	105

TABLE 2. Description of parameters of simulations.

A different configuration was selected for the present study. Here an *initially laminar lean flame* was established and propagated into a non-homogeneous turbulent mixture having the *same global lean stoichiometry*. This corresponds more closely to conditions in a stratified-charge direct injection engine at part-load, low-speed operation. In a globally lean mixture, where the distribution of local reaction rates is symmetric about the mean the mean reaction rate per unit flame length would be similar in homogeneous and non-homogeneous cases (see Fig. 1). This combined with an increase in flame length would result in the global heat release being higher in the non-homogeneous case. Here different distributions about the mean were explored to establish the effects in efficiency of combustion and NO formation. In a first simulation (B1 in table 1), mixture inhomogeneities were symmetrically distributed around the mean and thus limited to $\Delta\phi = \pm.6$. Results showed a small gain in heat release as compared to homogeneous combustion (see Fig. 2), as only a small portion of the mixture was close to stoichiometric or rich. A second configuration (C1) was designed in which inhomogeneities were introduced in an asymmetrical way with a thinner but higher peak towards the rich side. This is expected to correspond more closely to conditions in an engine, where fuel is injected as a liquid. Case C1 presented a clear gain in efficiency (see Fig. 2) mainly due to a higher mean heat release per unit flame length, as total flame length was essentially the same as for the previous configuration (Fig. 2).

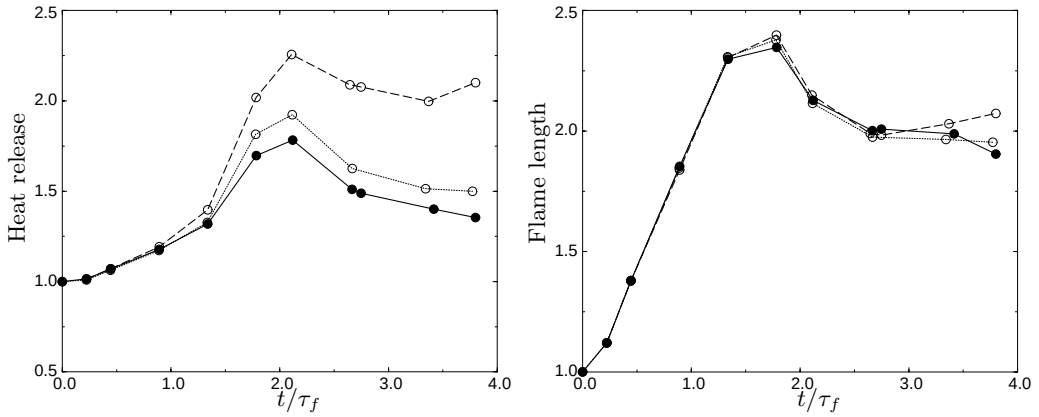

FIGURE 2. Global heat release (left) and flame length (right) of a lean ($\phi = .6$) flame propagating into a homogeneous lean mixture (–●–), a non-homogeneous mixture symmetrically distributed around $\phi = .6$ (–○–), and a non-homogeneous mixture biased to the rich side (- -○ - -). Values are normalized by those corresponding to a planar laminar flame with $\phi = .6$.

The simulations were initialized with reactants on one side of the computing domain and products on the other side, separated by a lean ($\phi = .6$) planar laminar premixed flame. Two-dimensional turbulence was imposed as an initial condition using an energy spectrum parametrized by the initial rms turbulent velocity u'_{T0} and the initial turbulence integral length scale l_{T0} or characteristic time τ_{T0} (Haworth & Poinsot, 1992). Other parameters are the initial turbulent Reynolds number Re_{T0}, the initial laminar flame propagation speed s_l^0, the initial laminar flame thickness δ_l^0, and the flame time τ_f, defined in Haworth *et al.*, 2000a as: $\tau_f = 2\delta_l^0/(s_l^0(1+\rho_u/\rho_b))$. The values of these parameters for the present simulations are reported in table 2. The different simulations performed differ only in the length scales λ_ϕ and ranges of equivalence ratio imposed as initial conditions (table 1).

The chemical mechanism adopted was a 28-species 73-reaction propane mechanism proposed in Haworth *et al.*, 2000a to which two additional species (N and NO) and three reactions were added for thermal NO (extended Zeldovich mechanism). Chemistry parameters for the NO mechanism were taken from Hanson and Salimian, 1984.

4. Primary flame characterization

The computed fuel mass fraction and heat release fields corresponding to times $t/\tau_f = 2$ and $t/\tau_f = 4$ obtained in three simulations (A, C1, and C2) are shown in Fig. 3. Also shown are the stoichiometric contour line of the mixture fraction field z_{C+H} and contours of the progress variable c, defined as (Haworth *et al.*, 2000a):

$$z_{C+H} = \sum_{n=1}^{Nspecies} (Y_C^n + Y_H^n), \qquad c = 1 - Y_{C3H8}/z_{C+H}.$$

Case A corresponds to a homogeneous reactant mixture with equivalence ratio $\phi = .6$, case C1 to a non-homogeneous reactant mixture in which the initial length scale of inhomogeneities is $\lambda_\phi = 1$, and case C2 to a non-homogeneous mixture with λ_ϕ=4. The same initial turbulence was imposed in the three cases. At time $t/\tau_f = 2$ the flame front displays the same shape in all three cases, while differences are apparent by time $t/\tau_f = 4$. Locally different propagation speeds due to inhomogeneities have deformed the

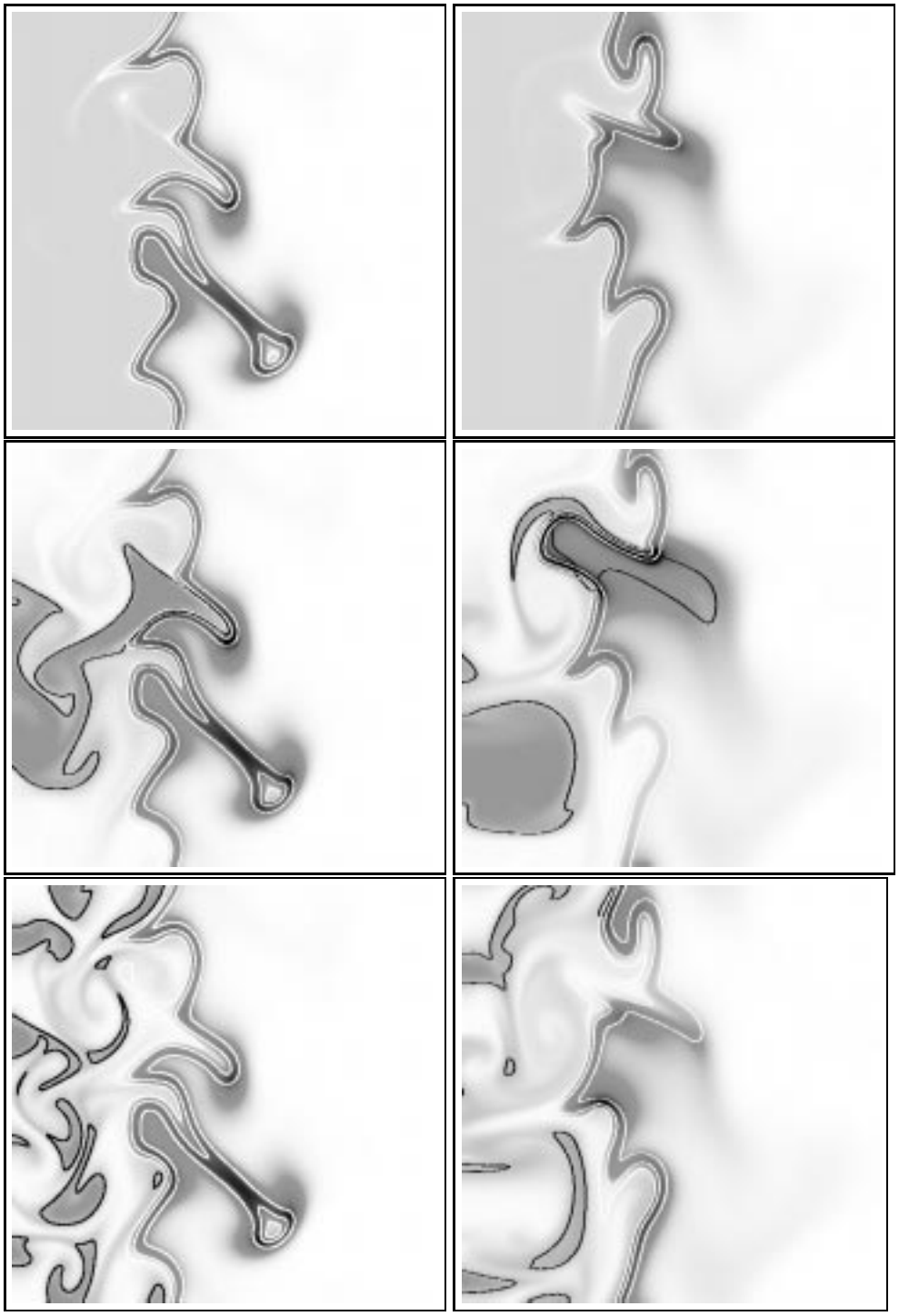

FIGURE 3. Heat release (marked by white lines representing progress variable isocontours) and fuel mass fraction (marked by black line representing the stoichiometric isocontour) fields. Results correspond to times $t/\tau_f = 2$ (left) and $t/\tau_f = 4$ (right) and to r A (top), C1 (middle), and C2 (bottom) simulations. Scale goes from white at zero values to light grey for fuel mass fraction and to black for heat release.

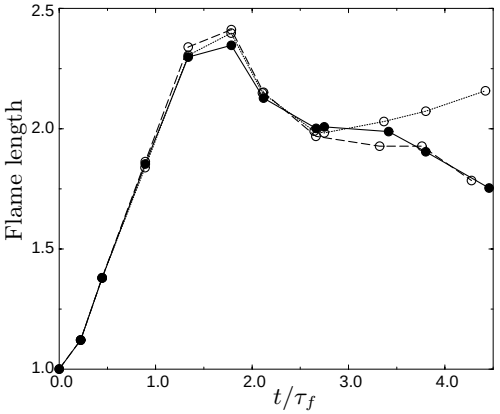

FIGURE 4. Time evolution of flame length in A (–●–), C1 (–○–) and C2 (- -○- -).

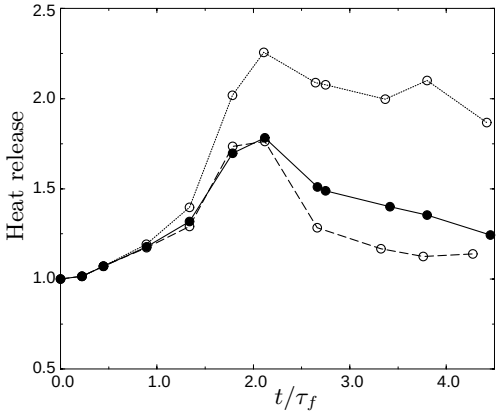

FIGURE 5. Time evolution of global heat release in A (–●–) C1, (–○–) and C2 (- -○- -).

flame front in C1 at the later time, resulting in a longer flame compared to flame A. The flame front is only slightly deformed in simulation C2 as a result of the smaller size of the rich/lean pockets.

Time evolution of the flame length, computed as the length of a progress variable iso-contour ($c = 0.9$), is plotted in Fig. 4. Time is normalized in this figure by the flame time τ_f, and flame length is normalized by the length of the initial laminar planar lean ($\phi = .6$) flame. All three flames present a similar initial increase in length up to time $t/\tau_f = 1.25$, where they all reach twice their initial length. This similar evolution suggests that turbulent wrinkling dominates at this stage. Later, small differences in length appear, with the non-homogeneous flames growing faster than the homogeneous one. These are the first signs of the effect of non-homogeneities and are too small to be visible in Fig. 3. Flame length then decreases in all three cases, probably as the pocket visible in Fig. 3 at time 2 is consumed. At late times flame C1 clearly separates from the other two, presenting a net increase in flame length corresponding to a rapidly propagating close-to-stoichiometric/rich flame segment that can be identified in Fig. 3 in the upper third of C1. Flames A and C2 continue to have similar lengths as expected from the lack of deformation of flame C2.

Figure 5 displays the evolution of global heat release for the same simulations. Heat release is computed by integrating the local heat release over the computational domain and normalizing by the heat release of the initial planar laminar lean ($\phi = .6$) flame. Its rate of increase is smaller than that of flame length; by time 1.25 it has reached only 1.25 times its initial value in all cases. Differences in global heat release increase become significant after this time, with flame C1 increasing much more rapidly than the other two. Since flame length is identical for all three flames up to times > 3, this different behavior must be due to locally greater heat release per unit flame length in C1.

Mean heat release per unit flame length is plotted in Fig. 6. At early times the same decreasing tendency is seen for all three flames, which must be associated with turbulent straining effects. The effects of higher local equivalence ratio in the C1 case begin to dominate after some time. This delay is due to the initial conditions: there is a separation between the initial flame front and the region where non-homogeneities are introduced to avoid numerical problems. The flame must propagate across this separation to reach the rich/lean pockets. In case C2 the mean heat release follows the same trend as in the homogeneous case. While cases C2 and C1 initially have the same mean and fluctuation

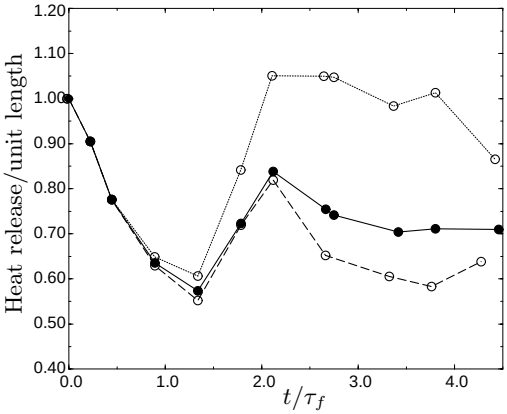

FIGURE 6. Time evolution of mean heat release per unit flame length in A (–●–), C1 (–○–) and C2 (- -○- -).

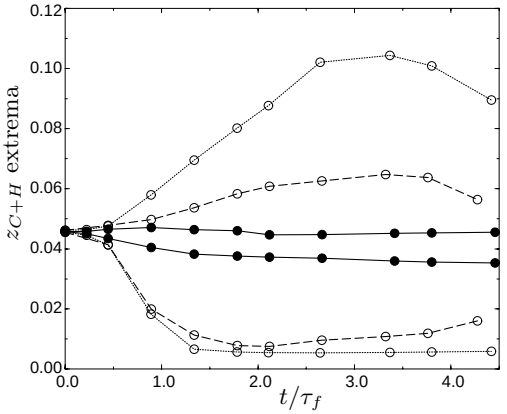

FIGURE 7. Time evolution of the maxima and minima of z_{C+H} on the $c = .9$ isocontour in A (–●–), C1 (–○–) and C2 (- -○- -).

in the equivalence ratio distribution, the smaller length scales of case C2 make turbulent mixing more effective in bringing the mixture towards homogeneity; by the time the flame front reaches the non-homogeneous region, the equivalence ratio fluctuations have been damped.

A somewhat surprising effect is observed at the latest times, where the mean heat release for simulation C2 is even smaller than that of the homogeneous case. This can be explained by local extinction effects in extreme lean zones (see Fig. 3), which are much more important in C2 than in C1. Although the global initial distribution of rich/lean zones is the same for flames C1 and C2 and they eventually evolve towards the same final distribution, the evolution of the distribution on the flame front is quite different. In Fig. 7 the time evolutions of the maximum and minimum values of z_{C+H} at the flame front (given by the $c = 0.9$ isocontour) are plotted for the three simulations. The distribution is clearly shifted to lean values for all three cases, but in C1 it is shifted later to rich values. The effect of shifting towards leaner values is to reduce the mean heat release per unit length, and this could be the explanation for the more important decrease in mean heat release seen in case C2.

This shifting effect was already observed in Poinsot *et al.*, 1996. There it was attributed to a longer residence time, thus a larger probability of occurrence of lean pockets as compared to rich ones due to smaller flame speeds. In the present simulation, this effect is larger for the C2 case as it is probably enhanced by the asymmetrical small-scale initial distribution of inhomogeneities there with richer pockets smaller than lean pockets, thus mixing more rapidly. In case C1, where scales of inhomogeneity are larger, mixing effects are less important and the shift towards leaner values can intermittently be compensated by rich pockets arriving at the flame front (Fig. 7).

5. Post flame characterization

The secondary reaction zone is usually defined by means of the progress variable c as the zone in which primary fuel has totally disappeared ($c > .9999$ or even $c = 1$). As in previous studies, it was found that only a very small portion of the global heat release occurs in this post-primary flame zone. The most important secondary reaction zone in the present simulations, corresponding to case C1, can be seen in Fig. 3 behind the richer

flame segment and close to the stoichiometric line, and represents a very small percentage of the total heat release. In simple chemistry, the fact that the flame is located near the stoichiometric line would directly suggest a diffusion flame, but in complex chemistry this is much more difficult to establish. The secondary flame reactants are not the original reactants, but are species derived from them. The stoichiometric line represents the line at which the C+H and O concentration are in the same proportions as if there were 5 moles of O_2 and 1 of C_3H_8, so that in the global reaction $C_3H_8 + 5O_2 = 3CO_2 + 4H_2O$ they would be totally consumed to produce 3 moles of CO_2 and 4 of H_2O.

But there is no propane in the secondary reaction zone, and the reactions that do occur there do not have the same stoichiometry as the global reaction. Reaction close to global stoichiometry occurs between products of the rich zone (that is, products derived from propane cracking) and products of the lean zone (mainly O and O_2), but does not imply that they are mixed or unmixed.

In Fig. 8 we have tried to illustrate the post flame structure by plotting the mass fractions and production rates of some representative species. All figures correspond to simulation C1 and time $t/\tau_f = 4$, and production rates are plotted so that negative rates are always white and positive rates black. The grey background represents zero net production rate, and the scale has been chosen to allow a better visualization of the secondary flame (it is not linear). The scale for mass fraction is linear with white representing minimum values and black maximum values. The stoichiometric line shows the separation between rich zones in which excess H_2 and CO are found and lean zones in which excess O_2 is found. In examining secondary reaction production rates, it can be seen that O_2 is consumed at the stoichiometric line, suggesting a diffusion flame structure. But for other species reaction is occurring also in other zones: H_2 is consumed right on the stoichiometric line but is then produced in the region delimited by this line, that is, in the rich zone; CO is also consumed in the rich zone. Then H_2 is probably reacting with O_2 in a non-premixed mode, but there are other reactions in which H_2 and CO are involved (as well as other species not shown), occurring in a premixed mode. No clear description in terms of a classical diffusion flame can be depicted for this secondary reaction; in fact, many reactions of different stoichiometries are occurring in the post flame region, and probably some occur in a premixed mode and others in a non-premixed mode.

6. NO formation

NO formation occurs at higher temperatures than those of the primary flame and thus mainly in the post-flame region. Production of NO is enhanced in the non-homogeneous lean cases, as compared to the homogeneous lean case, as higher temperatures and concentrations of O atoms are reached. Figure 9 displays the time evolution of the total mass of NO for simulations A (homogeneous), C1 (non-homogeneous large-scale), and C2 (non-homogeneous small-scale). NO mass is higher in both non-homogeneous cases compared to the homogeneous one, but significant differences exist as well between the two non-homogeneous simulations. While NO mass in case C1 reaches a value 40% higher than in the homogeneous case, in case C2 it is only 5% higher. Higher heat release rates are giving much higher local temperature values in the C1 case compared to C2, which together with higher O concentrations explains this enhanced production effect.

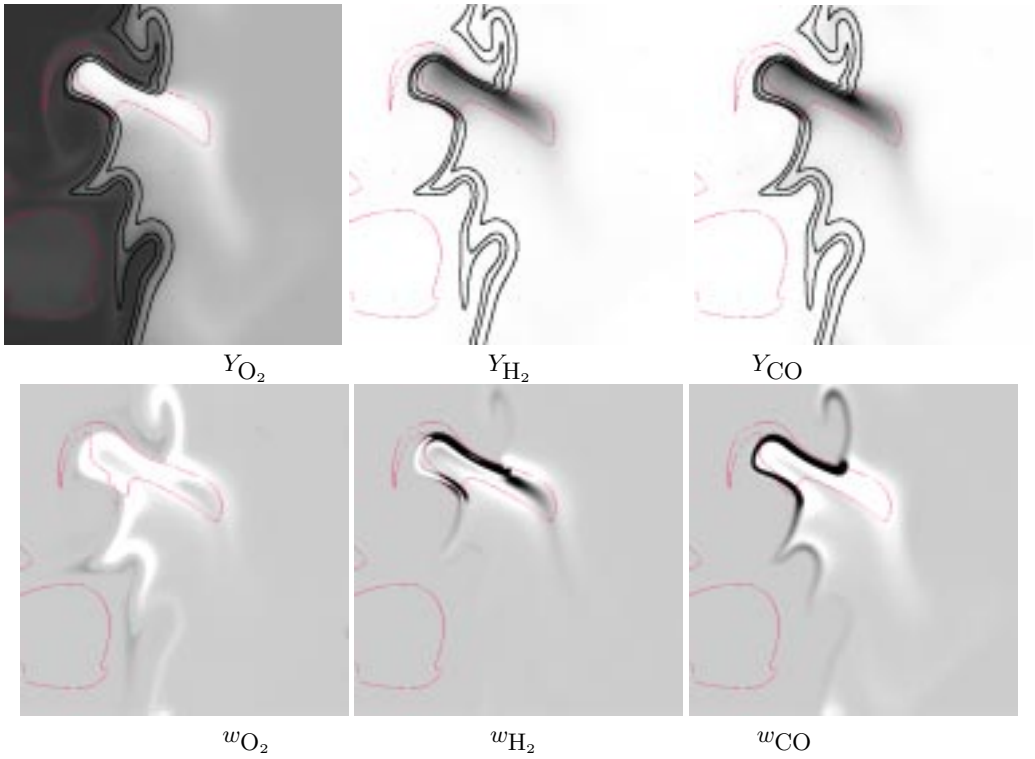

FIGURE 8. Mass fractions (top) and production rates (bottom) of O_2 (left), H_2 (middle) and CO (right) corresponding to C1 at $t/\tau_f = 4$. For reaction rates white represents negative values and black positive values, background grey corresponds to zero net production, and the scale is adapted to emphasize secondary reactions. For mass fractions white represents minimum and black maximum values, and the scale is linear.

7. A test for the flamelet assumption

A simple new test concerning the modeling of the primary flame has been performed in this work by directly comparing the heat release obtained in the DNS with that predicted by a flamelet model. It is usually accepted that a variable equivalence ratio premixed flamelet assumption is well suited for partially premixed combustion, but quantitative testing of this assumption was not feasible with previous DNS results as no significant differences between heat release in non-homogeneous and homogeneous flames were found.

A simplified formulation of this modeling assumption has been adopted here: The turbulent flame is assumed to be locally equivalent to an unstrained premixed laminar flamelet with the same z_{C+H}. By using a library for the heat release associated with a premixed laminar flamelet as a function of mixture fraction $h(z_{C+H})$, modeled heat release was computed as the integral of $h(z_{C+H})$ along a progress variable isocontour $c = c^*$:

$$H = \int_{c=c*} h(z_{C+H}) d\Sigma_{c=c*}.$$

Results of this computation are compared in Fig. 10 to the results of DNS for the homogeneous (A) and the non-homogeneous (C1) cases. The model appears to predict the global heat release remarkably well. Differences at initial times probably are due to the dismissal of strain-rate effects. In Fig. 6 it has been shown that at early times

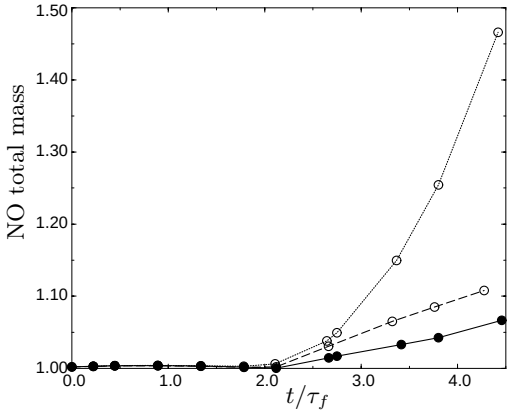

FIGURE 9. Time evolution of NO global mass in A (–●–), C1 (–○–) and C2 (- -○- -) simulations.

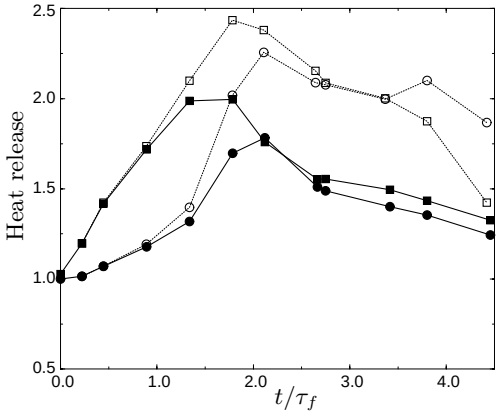

FIGURE 10. Computed and modeled global heat release for cases A (● computed, ■ modeled value) and C1 (○ computed and □ modeled value).

effects of turbulent strain rate are very important in reducing the mean heat release per unit flame area. Using an unstrained flamelet to compute heat release gives a too-high estimation for the local heat release and results in a high global heat release. Later, the model appears to correctly predict the heat release in both cases, but at the latest times there is an appreciable departure in the non-homogeneous case, with the model predicting a heat release about 60% smaller than that given by simulations.

This could be an effect of temperature mixing: at late times in the non-homogeneous case, temperature may have diffused from locally stoichiometric high-temperature zones to locally leaner or richer zones. The higher temperature may make some flame segments burn fast compared to the equivalent laminar flame. On examination of the picture corresponding to late times in the C1 simulation in Fig. 3, one finds that the high heat release zone corresponding to the stoichiometric reactants is, in fact, extended far beyond the stoichiometric line to reach leaner and richer flame zones. This is an effect that a flamelet model based only on the local equivalence ratio will not be able to predict.

8. Conclusions

Simulations of combustion in a stratified premixed propane-air mixture have been performed under global lean conditions, approaching those of a gasoline direct injection (GDI) engine. Detailed transport, thermodynamics, and chemistry, including thermal NO production, were included, which suggests high reliability of results. However, the low Reynolds number and the two-dimensionality of the turbulence demand some precaution in generalizing directly to practical combustion systems. Substantial differences in the amount of heat release between homogeneous and non-homogeneous reactants have been obtained. This has permitted a detailed study of the different phenomena affecting combustion efficiency in partially premixed systems. In particular, a strong influence of the spatial distribution of the nonhomogeneities on heat release and NO formation was found. Moreover, a quantitative assessment of flamelet models for the primary flame has been made, yielding excellent agreement. A qualitative study of the secondary reaction zone has shown the difficulties that a flamelet interpretation would present.

REFERENCES

Baum, M., Poinsot, T., Haworth, D., & Darabiha, N. 1994 Direct numerical simulation of $H_2/O_2/N_2$ flames with complex chemistry in two-dimensional turbulent flows. *J. Fluid Mech.* **281,** 1-32.

Glassman, I. 1987 *Combustion.* Academic Press.

Hanson, R. K. & Salimian, S. 1984 *Combustion Chemistry.* Springer-Verlag.

Haworth, D., Blint, R., Cuenot, B., & Poinsot, T. 2000 Numerical simulation of turbulent propane-air combustion with non-homogeneous reactants. *Comb. Flame.* **121,** 395-417.

Haworth, D., Cuenot, B., Poinsot, T. & Blint, R. 2000 Direct numerical simulation of turbulent propane-air combustion with non-homogeneous reactants. In *Eighth International Conference on Numerical Combustion, Amelia Island, FL.*

Haworth, D., & Poinsot, T. 1992 Numerical simulations of Lewis number effects in turbulent premixed flames. *J. Fluid Mech.* **244,** 405-436.

Hélie, J. & Trouvé, A. 1998 Turbulent flame propagation in partially premixed combustion. *27th Symposium (Int.) on Combustion.*

Kee, R. J., Miller, J. A. & Jefferson, T. H. 1980 Chemkin: a general-purpose, problem-independent, transportable FORTRAN chemical-kinetics package. *SANDIA Tech. Report: SAND 83-8003.*

Kee, R. J., Warnatz, J. & Miller, J. A. 1983 A FORTRAN computer code package for the evaluation of gas-phase viscosities, conductivities and diffusion coefficients. *SANDIA Tech. Report: SAND 83-8209.*

Krieger, R. B., Siebert, R. M., Pinson, J. A., Gallopoulos, N. E., Hilden, D. L., Monroe, D. R., Rask, R. B., Solomon, A. S. P, & Zima, P. 1997 Diesel engines: one option to power future personal transportation vehicles. *SAE paper no. 972683.*

Légier, J. P., Poinsot, T., Veynante, D., & Nicoud, F. 2000 Dynamically thickened flame LES model for premixed and non-premixed combustion. *Proc. Summer Program,* Center for Turbulence Research, NASA Ames/Stanford Univ., this volume.

Lele, S. K. 1992 Compact finite difference schemes with spectral-like resolution. *Journal of Computational Physics.* **103,** 16-42.

Peters, N. 2000 *Turbulent Combustion.* Cambridge Univ. Press.

Poinsot, T., Veynante, D., Trouvé, A., & Ruetsch, G. 1996 Turbulent flame propagation in partially premixed flames. *Proc. Summer Program*, Center for Turbulence Research, NASA Ames/Stanford Univ. 111-136.

Takagi, Y. 1998 A new era in spark-ignition engines featuring high-pressure direct injection. *27th Symposium (Int.) on Combustion.*

Zhao, F. Q., Lai, M. C., & Harrington, D. L. 1999 Automotive spark-ignited direct-injection gasoline engines. *Prog. Energy Combust. Sci.* **25**, 437-562.

Zhou, J., Nishida, K., Yoshikazi, T. & Hiroyasu, H. 1998 Flame propagation characteristics in a heterogeneous concentration distribution of a fuel-air mixture. *SAE paper no. 982563.*